ELSEVIER

Comput. Methods Appl. Mech. Engrg. 191 (2002) 4851–4867

Computer methods in applied mechanics and engineering

www.elsevier.com/locate/cma

Convergence of the domain decomposition finite element–boundary element coupling methods

M. El-Gebeily [a,*], Wael M. Elleithy [b], Husain J. Al-Gahtani [c]

[a] *Department of Mathematical Sciences, King Fahd University of Petroleum and Minerals, Dhahran 31261, Saudi Arabia*
[b] *Department of Mechanical Systems Engineering, Faculty of Engineering, Shinshu University, Nagano 380-8553, Japan*
[c] *Department of Civil Engineering, King Fahd University of Petroleum and Minerals, Dhahran 31261, Saudi Arabia*

Received 8 February 2001; received in revised form 23 December 2001; accepted 4 June 2002

Abstract

In this work, we analyze three available domain decomposition methods. We also establish the convergence conditions. The theoretical analysis provides an interval in which a relaxation parameter has to be chosen in order to achieve convergence. Moreover, it allows the selection of the relaxation parameter so that convergence is achieved with the minimum number of iterations. Several example problems are given for elaboration.

Keywords: Finite element method; Boundary element method; Domain decomposition; Coupling; Convergence

1. Introduction

Coupling the finite element method (FEM) and the boundary element method (BEM) is well known as an effective analysis and numerical tool, which makes use of their individual merits. The conventional coupling scheme employs an entire unified equation for the whole domain, by combining the discretized equations for the BEM and FEM sub-domains. The reader may refer to Refs. [1–8], not to mention many others. However, the algorithm for constructing an entire equation for the whole domain is highly complicated when compared with that for each single equation. In recent years, coupling the BEM and the FEM has been achieved through the domain decomposition methods [9–13]. In these coupling methods there is no need to combine the coefficient matrices of the FEM and the BEM sub-domains, as is required in the conventional coupling methods. Instead, separate computing for each sub-domain and successive renewal of the variables on the interface for both sub-domains are performed to reach the final convergence.

Although, the domain decomposition coupling methods offer some advantages over other methods, some important issues related to the convergence of the iterative solution need to be addressed. The objective of this paper is to derive the convergence conditions of three available iterative domain

* Corresponding author.
E-mail addresses: mgebeily@kfupm.edu.sa (M. El-Gebeily), elleithy@homer.shinshu-u.ac.jp (W.M. Elleithy).

0045-7825/02/$ - see front matter
PII: S0045-7825(02)00405-X

decomposition-coupling methods. The condition for obtaining a value of the relaxation parameter to speed up convergence is also derived. The importance of the choice of the relaxation parameter is also demonstrated.

2. Preliminaries

Consider the 2-D problem of Fig. 1, which is modeled using the BEM and FEM. The corresponding boundary integral equation for the BEM sub-domain is given by:

$$\begin{bmatrix} H_{11} & H_{12} \\ H_{21} & H_{22} \end{bmatrix} \begin{bmatrix} u_B^B \\ u_B^I \end{bmatrix} = \begin{bmatrix} G_{11} & G_{12} \\ G_{21} & G_{22} \end{bmatrix} \begin{bmatrix} q_B^B \\ q_B^I \end{bmatrix}, \tag{1}$$

where u and q are column matrices containing the boundary nodal values for the potential (Dirichlet data) and the flux (Neumann data), respectively. H and G are influence coefficient matrices. For the FEM sub-domain, the assembled element equations take the form:

$$\begin{bmatrix} K_{11} & K_{12} \\ K_{21} & K_{22} \end{bmatrix} \begin{bmatrix} u_F^F \\ u_F^I \end{bmatrix} = \begin{bmatrix} f_F^F \\ f_F^I \end{bmatrix}, \tag{2}$$

where K is the stiffness matrix for the system, and u and f are the nodal potentials and integrated flux vectors respectively. At the interface, the compatibility and equilibrium conditions are:

$$u_B^I = u_F^I \in \Gamma^I, \tag{3}$$

$$f_F^I + Mq_B^I = 0 \in \Gamma^I, \tag{4}$$

where M is the converting matrix due to the weighing of the boundary fluxes by the interpolation function on the interface.

In Sections 2.1–2.3 we are going to discuss three available domain decomposition schemes for coupling the FEM and BEM.

2.1. Sequential Schwarz Dirichlet–Neumann scheme

The sequential Dirichlet–Neumann domain decomposition method may be described as follows [11,12]:

1. Set initial guess $u_{B,0}^I = \bar{u}$
2. Do for $n = 0, 1, 2, \ldots$ until convergence

$$\text{solve} \begin{bmatrix} H_{11} & H_{12} \\ H_{21} & H_{22} \end{bmatrix} \begin{bmatrix} u_B^B \\ u_{B,n}^I \end{bmatrix} = \begin{bmatrix} G_{11} & G_{12} \\ G_{21} & G_{22} \end{bmatrix} \begin{bmatrix} q_B^B \\ q_{B,n}^I \end{bmatrix} \quad \text{for } q_{B,n}^I, \tag{5}$$

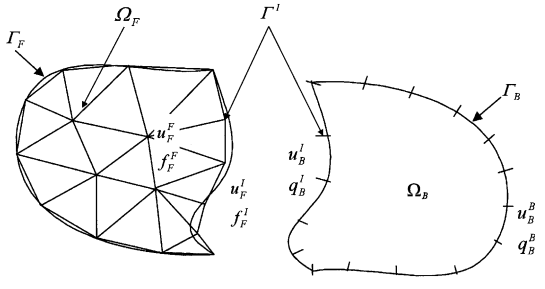

Fig. 1. Domain decomposed into FEM and BEM sub-domains.

$$\text{solve} \begin{bmatrix} K_{11} & K_{12} \\ K_{21} & K_{22} \end{bmatrix} \begin{bmatrix} u_F^F \\ u_{F,n}^I \end{bmatrix} = \begin{bmatrix} f_F^F \\ -Mq_{B,n}^I \end{bmatrix} \quad \text{for } u_{F,n}^I, \tag{6}$$

$$\text{apply } u_{B,n+1}^I = (1-\gamma)u_{B,n}^I + \gamma u_{F,n}^I, \tag{7}$$

where γ is a relaxation parameter to ensure and/or accelerate convergence.

2.2. Parallel Schwarz Dirichlet–Neumann scheme

In this scheme [10], the initial assumed data on the interface for the BEM sub-domain is the Dirichlet data, while that for the FEM sub-domain is the Neumann data. The computations for FEM and BEM are performed in parallel. The method may be described as follows:

1. Set initial guess $u_{B,0}^I = \bar{u}$ and $q_{F,0}^I = \bar{q}$
2. Do for $n = 0, 1, 2, \ldots$ until convergence

$$\text{solve} \begin{bmatrix} H_{11} & H_{12} \\ H_{21} & H_{22} \end{bmatrix} \begin{bmatrix} u_B^B \\ u_{B,n}^I \end{bmatrix} = \begin{bmatrix} G_{11} & G_{12} \\ G_{21} & G_{22} \end{bmatrix} \begin{bmatrix} q_B^B \\ q_{B,n}^I \end{bmatrix} \quad \text{for } q_{B,n}^I, \tag{8}$$

$$\text{solve} \begin{bmatrix} K_{11} & K_{12} \\ K_{21} & K_{22} \end{bmatrix} \begin{bmatrix} u_F^F \\ u_{F,n}^I \end{bmatrix} = \begin{bmatrix} f_F^F \\ Mq_{F,n}^I \end{bmatrix} \quad \text{for } u_{F,n}^I, \tag{9}$$

$$\text{apply } u_{B,n+1}^I = (1-\alpha)u_{B,n}^I + \alpha u_{F,n}^I, \tag{10}$$

$$\text{apply } q_{F,n+1}^I = -q_{B,n}^I, \tag{11}$$

where α is a relaxation parameter to ensure and/or accelerate convergence.

2.3. Parallel Schwarz Neumann–Neumann scheme

In this scheme, the Neumann data is assumed in advance both on the interface of the FEM and BEM sub-domains [9]. The domain decomposition coupling method can be described as follows:

1. Set initial guess $q_{B,0}^I = \bar{q}$ and $q_{F,0}^I = -q_{B,0}^I$
2. Do for $n = 0, 1, 2, \ldots$ until convergence

$$\text{solve} \begin{bmatrix} H_{11} & H_{12} \\ H_{21} & H_{22} \end{bmatrix} \begin{bmatrix} u_B^B \\ u_{B,n}^I \end{bmatrix} = \begin{bmatrix} G_{11} & G_{12} \\ G_{21} & G_{22} \end{bmatrix} \begin{bmatrix} q_B^B \\ q_{B,n}^I \end{bmatrix} \quad \text{for } u_{B,n}^I, \tag{12}$$

$$\text{solve} \begin{bmatrix} K_{11} & K_{12} \\ K_{21} & K_{22} \end{bmatrix} \begin{bmatrix} u_F^F \\ u_{F,n}^I \end{bmatrix} = \begin{bmatrix} f_F^F \\ Mq_{F,n}^I \end{bmatrix} \quad \text{for } u_{F,n}^I, \tag{13}$$

$$\text{apply } q_{B,n+1}^I = q_{B,n}^I + \beta\left(u_{F,n}^I - u_{B,n}^I\right), \tag{14}$$

$$\text{apply } q_{F,n+1}^I = -q_{B,n}^I, \tag{15}$$

where β is a relaxation parameter ensure and/or accelerate convergence.

3. Convergence and optimal convergence of the iterative schemes

In this section we are going to establish the convergence and optimal convergence conditions for the three domain decomposition methods described in Section 2.

3.1. Sequential Schwarz Dirichlet–Neumann scheme

After applying boundary conditions and rearranging, Eq. (5) can be written in the following form

$$\begin{bmatrix} X_B^B \\ q_{B,n}^I \end{bmatrix} = \begin{bmatrix} A_{11} & A_{12} \\ A_{21} & A_{22} \end{bmatrix} \begin{bmatrix} C_B \\ u_{B,n}^I \end{bmatrix}, \tag{16}$$

where X_B^B are the boundary unknowns in the BEM sub-domain except on the interface. Similarly one can apply boundary conditions and rearrange Eq. (6) to obtain:

$$\begin{bmatrix} u_F^F \\ u_{F,n}^I \end{bmatrix} = \begin{bmatrix} F_{11} & F_{12} \\ F_{21} & F_{22} \end{bmatrix} \begin{bmatrix} C_F \\ -Mq_{B,n}^I \end{bmatrix}. \tag{17}$$

Note that C_B and C_F are vectors of known values. Eliminating u_F^F from Eq. (17) yields:

$$u_{F,n}^I = F_{21}C_F - F_{22}Mq_{B,n}^I. \tag{18}$$

Using Eqs. (16) and (18) and substituting in Eq. (7) gives:

$$u_{B,n+1}^I = [(1-\gamma)I + \gamma T]u_{B,n}^I + \gamma Q, \tag{19}$$

where $T = -F_{22}MA_{22}$ and $Q = F_{21}C_F - F_{22}MA_{21}C_B$.

The eigenvalues of the system (19) are:

$$\theta_k = (1-\gamma) + \gamma\lambda_k, \tag{20}$$

where λ_k is the kth eigenvalue of T and $k = 1, 2, 3, \ldots, n$.

Lemma 1. *There exists a γ_c, such that $|\theta_k| < 1$ if and only if $Re(\lambda_k) < 1$.*

Proof. Notice that, for $\gamma \geqslant 0$, θ_k is on the line segment joining the points 1, λ_k in the complex plane. Fig. 2 shows two cases of λ_k, one with $\mathrm{Re}(\lambda_k) \geqslant 1$ and the other with $\mathrm{Re}(\lambda_k) < 1$. From this figure, it is clear that the assertion of the lemma holds iff $\mathrm{Re}(\lambda_k) < 1$. □

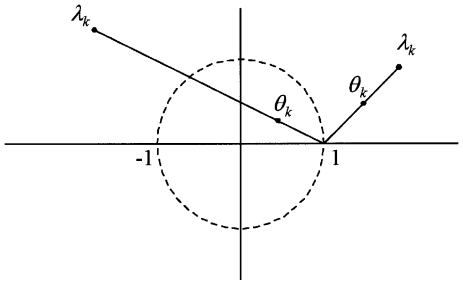

Fig. 2. The position of θ_k on the line joining 1 and λ_k.

For a suitable choice of γ, let $\lambda_k = x_k + \mathrm{i}y_k$, then (20) gives:

$$\left[x_k - \left(1 - \frac{1}{\gamma}\right)\right]^2 + y_k^2 < \frac{1}{\gamma^2}$$

which simplifies to:

$$(1 - x_k)^2 + y_k^2 < \frac{2(1 - x_k)}{\gamma}. \tag{21}$$

Inequality (21) immediately implies:

$$\gamma < \min_{1 \leqslant k \leqslant n} \left\{ \frac{2(1 - x_k)}{(1 - x_k)^2 + y_k^2} \right\}. \tag{22}$$

Next, we show that, there is a choice of the iteration parameter γ that minimizes the spectral radius of the iteration matrix $[(1 - \gamma)I + \gamma T]$. To obtain an optimum γ we must minimize:

$$\max_{1 \leqslant k \leqslant n} |(1 - \gamma) + \gamma\lambda_i|$$

which may be thought of as minimizing $\|C(\gamma)\|_\infty$
where

$$C(\gamma) = \begin{bmatrix} (1 - \gamma) + \gamma\lambda_1 \\ (1 - \gamma) + \gamma\lambda_2 \\ \vdots \\ (1 - \gamma) + \gamma\lambda_n \end{bmatrix}.$$

Since $\|x\|_\infty$ is not a differentiable function, we use the fact that

$$\frac{1}{\sqrt{n}}\|x\|_2 \leqslant \|x\|_\infty \leqslant \|x\|_2 \tag{23}$$

and minimize $\|C(\gamma)\|_2$ instead. Of course the optimum value for γ in $\|\cdot\|_2$ may not coincide with the optimum value in $\|\cdot\|_\infty$. Nevertheless, it bounds the latter one by virtue of (23). Let

$$F(\gamma) = \|C(\gamma)\|_2^2$$

then

$$F'(\gamma) = 2\sum_{k=1}^{n} \mathrm{Re}(\lambda_k - 1) + 2\gamma \sum_{k=1}^{n} |\lambda_k - 1|^2 \tag{24}$$

and

$$F''(\gamma) = 2\sum_{k=1}^{n} |\lambda_k - 1|^2 > 0,$$

i.e., the critical value of $\overline{\gamma}$ of (24) corresponds to a minimum.

$$\overline{\gamma} = -\frac{\sum_{k=1}^{n} \mathrm{Re}(\lambda_k - 1)}{\sum_{k=1}^{n} |\lambda_k - 1|} \tag{25}$$

and

$$F_{\min} = F(\overline{\gamma}) = n - \frac{\left(\sum_{k=1}^{n} \mathrm{Re}(\lambda_k - 1)\right)^2}{\sum_{k=1}^{n} |\lambda_k - 1|^2}. \tag{26}$$

It follows that, if $F_{\min} < 1$, then $\rho((1 - \overline{\gamma})I + \overline{\gamma}T) < 1$ and convergence is achieved.

3.2. Parallel Schwarz Dirichlet–Neumann scheme

As in the previous section, one can obtain:

$$u^I_{B,n+1} = (1-\alpha)u^I_{B,n} - \alpha R u^I_{B,n-1} + \alpha S, \tag{27}$$

where

$$R = F_{22}MA_{22} \quad \text{and} \quad S = F_{21}C_F - F_{22}MA_{21}C_B.$$

In Eq. (27), let:

$$v_n = u_{n-1} \quad \text{and} \quad w_n = u_n.$$

Then the parallel Shwarz Dirichlet–Neumann scheme can be written as the one step difference system:

$$\begin{bmatrix} v_{n+1} \\ w_{n+1} \end{bmatrix} = \begin{bmatrix} 0 & I \\ -\alpha R & (1-\alpha)I \end{bmatrix} \begin{bmatrix} v_n \\ w_n \end{bmatrix} + \begin{bmatrix} 0 \\ \alpha S \end{bmatrix}. \tag{28}$$

The eigenvalues of the above iteration matrix satisfy the equations:

$$\lambda^2 - (1-\alpha)\lambda + \alpha\lambda_k = 0, \quad k = 1, 2, 3, \ldots, n, \tag{29}$$

where $\lambda_1, \lambda_2, \lambda_3, \ldots, \lambda_n$ are the eigenvalues of R.

The solutions of the Eq. (29) are:

$$\theta^{\pm}_k = \frac{(1-\alpha) \pm \sqrt{(1-\alpha)^2 - 4\alpha\lambda_k}}{2}, \quad k = 1, 2, 3, \ldots, n.$$

To study the convergence of this scheme, we need the following lemma:

Lemma 2. *If $Re(\lambda_k) > -1$, then there exists an $\alpha_c > 0$ such that $|\theta^{\pm}_k| < 1$, $\forall \alpha \in [0, \alpha_c]$.*

Proof. Since $\theta^-_k(0) = 0$, then $\left|\theta^-_k(\alpha)\right| < 1$ is satisfied in some interval $[0, \alpha_c]$. We prove the statement of the lemma for $\theta^+_k(\alpha)$. Write $\theta^+_k = r + is$ and $\lambda_k = r_k + is_k$. Then

$$r^2 - s^2 - (1-\alpha)r + \alpha r_k = 0, \tag{30}$$

$$2rs - (1-\alpha)s + \alpha s_k = 0. \tag{31}$$

Now

$$\left.\frac{\mathrm{d}|\theta^+_k|}{\mathrm{d}\alpha}\right|_{\alpha=0} = \left.\frac{2rr' + 2ss'}{2\sqrt{s^2+r^2}}\right|_{\alpha=0}.$$

Since $r(0) = 1$ and $s(0) = 0$ then $\operatorname{sgn}\left(\frac{\mathrm{d}|\theta^+_k|}{\mathrm{d}\alpha}|_{\alpha=0}\right) = \operatorname{sgn}(r'(0))$. Differentiating (30) and setting $\alpha = 0$, we get:

$$r'(0) = -1 - r_k.$$

If $r_k > -1$, then $r'(0) < 0$, consequently $|\theta^+_k|$ is decreasing in a neighborhood of 0 and the conclusion follows. □

Remark. If $r_k < -1$ then $|\theta^+_k|$ is increasing in a neighborhood of 0. Since $|\theta^+_k(0)| = 1$, $|\theta^+_k(\alpha)| > 1$ in a neighborhood of 0.

The case of $r_k = 1$ and a sharper result will be treated in the next lemma, for the proof of which we need the following proposition.

Proposition 1. *Let $z = x + iy$ and $x, y \geqslant 0$. Then $Re\sqrt{z} \geqslant \sqrt{x}$, where, the branch $-\pi < \theta < \pi$ is taken for the square root function.*

Proof. Write $z = \sqrt{x^2+y^2}\,e^{i\theta}$, where $\theta = \tan^{-1}(y/x)$. The conditions $x \geqslant 0$, $y \geqslant 0$ and the branch taken for the square root function imply that $0 < \theta < \pi/2$.

$$\mathrm{Re}(\sqrt{z}) = (x^2+y^2)^{1/4}\cos\left(\frac{1}{2}\tan^{-1}\frac{y}{x}\right) = \sqrt{\frac{x+\sqrt{x^2+y^2}}{2}} \geqslant \sqrt{\frac{2x}{2}} = \sqrt{x}. \qquad \square$$

Lemma 3. *If $Re(\lambda_k) \leqslant -1$ then the numerical scheme is not convergent.*

Proof. Write $\lambda_k = r_k + is_k$, then the eigenvalues of the scheme are:

$$\theta_k^{\pm} = \frac{(1-\alpha) \pm \sqrt{(1-\alpha)^2 - 4\alpha r_k - 4\alpha i s_k}}{2} \quad \text{(we may assume wlog, that } s_k \geqslant 0\text{)}.$$

The condition $\mathrm{Re}(\lambda_k) \leqslant -1$ gives:

$$(1-\alpha)^2 - 4\alpha r_k \geqslant (1-\alpha)^2 + 4\alpha = (1+\alpha)^2.$$

Therefore, using Proposition 2, we get:

$$\mathrm{Re}\sqrt{(1-\alpha)^2 - 4\alpha r_k - 4\alpha i s_k} \geqslant \sqrt{(1-\alpha)^2 - 4\alpha r_k} \geqslant \sqrt{(1-\alpha)^2 + 4\alpha} = \sqrt{(1+\alpha)^2}.$$

So that $\mathrm{Re}(\theta_k^+) \geqslant (1/2)[(1-\alpha)+(1+\alpha)] = 1$ and $|\theta_k^+| \geqslant 1$.

The existence of an α that minimizes $\rho(A(\alpha))$ and a value for α, for which $\rho(A) = 1$, result from Lemma 2 and the fact that $\theta_k^- \to \infty$ as $\alpha \to \infty$. $\square$

3.3. Parallel Schwarz Neumann–Neumann scheme

As in 3.1 and 3.2, one can obtain:

$$u_{B,n+1}^I = (I - \beta C)u_{B,n}^I - \beta D u_{B,n-1}^I + \beta E, \tag{32}$$

where

$$C = A_{22}^{-1},$$

$$D = A_{22}^{-1}F_{22}MA_{22}$$

and

$$E = A_{22}^{-1}F_{21}C_F - A_{22}^{-1}F_{22}MA_{21}C_B.$$

As in Section 3.2 the parallel Shwarz Neumann–Neumann scheme can be written as the one step difference system:

$$\begin{bmatrix} v_{n+1} \\ w_{n+1} \end{bmatrix} = \begin{bmatrix} 0 & I \\ -\beta D & I - \beta C \end{bmatrix}\begin{bmatrix} v_n \\ w_n \end{bmatrix} + \begin{bmatrix} 0 \\ \beta E \end{bmatrix} \tag{33}$$

or

$$\xi_{n+1} = A(\beta)\xi_n + F(\beta). \tag{34}$$

For convergence we must have $\rho(A(\beta)) < 1$. The eigenvalues of $A(\beta)$ are roots of:

$$\det(\lambda(\lambda - 1)I + \lambda\beta C + \beta D) = 0. \tag{35}$$

The one-dimensional case will be considered here in order to illustrate the behavior of the spectral radius as β changes. The general case will be treated in the following section. Eq. (35) has the form:

$$\lambda^2 - (1 - \beta C)\lambda + \beta D = 0$$

and,

$$C, D > 0.$$

The roots of this equation are:

$$\lambda_1 = \frac{(1 - \beta C) + \sqrt{(1 - \beta C)^2 - 4\beta D}}{2}$$

and

$$\lambda_2 = \frac{(1 - \beta C) - \sqrt{(1 - \beta C)^2 - 4\beta D}}{2}.$$

The graphs of λ_1 and λ_2 against β are given in Fig. 3. In this figure, β_1 and β_2 are the values at which $(1 - \beta C)^2 - 4\beta D$ becomes zero. These values are:

$$\beta_1 = \left(\frac{\sqrt{C + D} - \sqrt{D}}{C}\right)^2$$

and

$$\beta_2 = \left(\frac{\sqrt{C + D} + \sqrt{D}}{C}\right)^2.$$

As depicted in Fig. 3, we remark that:

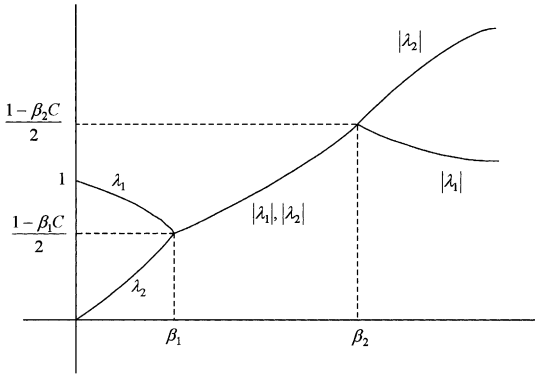

Fig. 3. $|\lambda|$ vs. β for the parallel Neumann–Neumann scheme.

$$1 > \frac{(1-\beta_1 C)}{2} = \frac{\sqrt{D}\sqrt{C+D}-D}{C} > 0,$$

$$\frac{(1-\beta_2 C)}{2} = -\frac{\sqrt{D}\sqrt{C+D}+D}{C} < 0$$

and

$$|1-\beta_2 C| > (1-\beta_1 C).$$

It follows that the minimum spectral radius is $(1-\beta_1 C)/2$ occurring at $\beta = \beta_1$. Note that $\rho(A(\beta_1)) < 1$ and the choice of $\beta = \beta_1$ corresponds to the fastest rate of convergence. We also note that as $\beta \to \infty$, $|\lambda_2| \to \infty$. Therefore at a certain β, the spectral radius becomes 1. This is the supremum of the allowable values for β which preserves the stability of the algorithm.

4. A unified convergence analysis

In this section we carry out a unified convergence analysis of the schemes presented in the previous two sections. The findings in this section are of a more general character than those of Section 3. For the purpose of analyzing convergence we will assume the form of the domain decomposition methods can be given in the following form:

$$u_{n+1} - u_n + \rho A u_n + \rho \Lambda u_{n-1} = 0, \tag{36}$$

where ρ is the relaxation parameter, i.e., one can define:

$A = I + T, \quad \Lambda = 0$ (sequential Dirichlet–Neumann domain decomposition coupling method),

$A = I, \quad \Lambda = R$ (parallel Dirichlet–Neumann domain decomposition coupling method),

and

$A = C, \quad \Lambda = D$ (parallel Neumann–Neumann domain decomposition coupling method).

Proposition 2. *Define the characteristic equation of the scheme* (36) *by*:

$$\det((\lambda^2 - \lambda)I + \lambda\rho A + \rho\Lambda) = 0. \tag{37}$$

Then we have the following properties:

(a) *The roots of* (37) *are the eigenvalues of the block matrix* $\begin{bmatrix} 0 & I \\ -\rho\Lambda & I-\rho A \end{bmatrix}$

(b) λ *is a root of* (37) *if and only if* $u_n = \lambda^n\gamma$ *is a solution of* (36) *for some nonzero vector* γ.

(c) *The system* (36) *is stable if and only if all roots of* (37) *have modulus less than one.*

Proof. (*a*) $\det\left(\lambda I - \begin{bmatrix} 0 & I \\ -\rho\Lambda & I-\rho A \end{bmatrix}\right) = \det\begin{pmatrix} \lambda I & -I \\ \rho\Lambda & (\lambda-1)I + \rho A \end{pmatrix} = \det((\lambda^2-\lambda)I + \lambda\rho A + \rho\Lambda).$

Suppose λ is a root of (37), Let γ be a nontrivial solution of $[(\lambda^2-\lambda)I + \lambda\rho A + \rho\Lambda]\gamma = 0$. Set $u_n = \lambda^n\gamma$. It can be easily checked that u_n satisfies (36). On the other hand, if $u_n = \lambda^n\gamma$ for some nontrivial γ, then:

$$[(\lambda^2-\lambda)I + \lambda\rho A + \rho\Lambda]\gamma = 0,$$

or

$$\det[(\lambda^2-\lambda)I + \lambda\rho A + \rho\Lambda]\gamma = 0,$$

i.e., λ is a root of (37).

(b) The system (36) can be put in the equivalent form:

$$u_{n+1} = \begin{bmatrix} 0 & I \\ -\rho\Lambda & I - \rho A \end{bmatrix} u_n \tag{38}$$

which is stable if and only if its eigenvalues have modulus less than one. By part (a), these are the same as the roots of (37). □

Let λ be a root of (36) and γ a nontrivial solution of $[(\lambda^2 - \lambda)I + \lambda\rho A + \rho\Lambda]\gamma = 0$ normalized such that $\|\gamma\| = 1$. Multiplying both sides by $\gamma^* = [\gamma]^t$, we get:

$$(\lambda^2 - \lambda) + \lambda\rho a + \rho b = 0, \tag{39}$$

where,

$$a = \gamma^* A\gamma \quad \text{and} \quad b = \gamma^* \Lambda\gamma. \tag{40}$$

Theorem 1.
(a) *If* $Re(a + b) > 0$, *then there exists a* $\rho^+ > 0$, *such that* $|\lambda| < 1$ *for all* $\rho \in (0, \rho^+)$.
(b) *If* $Re(a + b) < 0$, *then there exists a* $\rho^- < 0$, *such that* $|\lambda| < 1$ *for all* $\rho \in (\rho^-, 0)$.

Proof. (a) Assume $\mathrm{Re}(a + b) > 0$. The two roots of (39) are:

$$\lambda^+ = \frac{(1 - \rho a) + \sqrt{(1 + \rho a)^2 - 4\rho(a + b)}}{2} \tag{41}$$

and

$$\lambda^- = \frac{(1 - \rho a) - \sqrt{(1 + \rho a)^2 - 4\rho(a + b)}}{2}. \tag{42}$$

Since $\lambda^- = 0$ at $\rho = 0$, there exists a ρ'_λ such that $|\lambda^-| < 1$ for all $\rho \in (0, \rho'_\lambda)$.

On the other hand, $\lambda^+ = 1$ at $\rho = 0$. We want to show that there is an interval $(0, \rho^2_\lambda)$ such that $|\lambda^+| < 1$ for all $\rho \in (0, \rho^2_\lambda)$.

For this purpose, write $\lambda^+ = r + \mathrm{i}s$. The real part of (39) satisfies:

$$r^2 - s^2 - r(1 - \rho \mathrm{Re}\, a) + s\rho \mathrm{Im}\, a + \rho \mathrm{Re}\, b = 0. \tag{43}$$

Now $|\lambda^+|^2 = r^2 + s^2$ and $\mathrm{d}|\lambda^+|^2/\mathrm{d}\rho = 2r(\mathrm{d}r/\mathrm{d}\rho) + 2s(\mathrm{d}s/\mathrm{d}\rho)$. At $\rho = 0$, $r = 1$ and $s = 0$. Using this and differentiating (43) we get

$$\left.\frac{\mathrm{d}r}{\mathrm{d}\rho}\right|_{\rho=0} = -\mathrm{Re}(a + b) < 0.$$

Therefore, $\left.\frac{\mathrm{d}|\lambda^+|^2}{\mathrm{d}\rho}\right|_{\rho=0} < 0$, and $|\lambda^+|^2$ is decreasing in a neighborhood of 0. Then, there exists a $\rho^2_\lambda > 0$ such that $|\lambda^+| < 1$ for all $\rho \in (0, \rho^2_\lambda)$. Part b can be proved similarly. □

Corollary 1. *Suppose* $\lambda_1, \lambda_2, \ldots, \lambda_m$ *are the roots of* (37) *and* $\gamma_1, \gamma_2, \ldots, \gamma_m$ *are the corresponding vectors computed from* (38). *If* $\mathrm{Re}(\gamma_k^*(A + \Lambda)\gamma_k) > 0$ $(\mathrm{Re}(\gamma_k^*(A + \Lambda)\gamma_k) < 0)$ *for* $k = 1, 2, \ldots, m$, *then there exists a* $\bar\rho > 0$ $(\bar\rho < 0)$, *such that the system* (36) *is stable for all* $\rho \in (0, \bar\rho)$ *(all* $\rho \in (\bar\rho, 0)$*).*

Proof. If $\mathrm{Re}(\gamma_k^*(A + \Lambda)\gamma_k) > 0$ for $k = 1, 2, \ldots, m$, then it follows from Theorem 1 that there exist positive numbers $\rho_1, \rho_2, \ldots, \rho_m$ such that $|\lambda_k| < 1$ for all $\rho \in (0, \rho_k)$, $k = 1, 2, \ldots, m$. Take $\bar\rho = \min(\rho_1, \rho_2, \ldots, \rho_m)$. The other case can be shown similarly. □

Since the condition $\mathrm{Re}(\gamma_k^*(A+\Lambda)\gamma_k) > 0$ is not readily available to check, we can, instead, check the following condition.

Corollary 2. *Let $\Gamma = A + \Lambda$. If $\Gamma + \Gamma^t$ is positive definite (negative definite), then the conclusion of Corollary 1 holds.*

Proof. If $\Gamma + \Gamma^t$ is positive definite, then for any root λ of (37) and any corresponding vector γ we have:

$$\mathrm{Re}(\gamma^*(A+\Lambda)\gamma) = \gamma_1^t\Gamma\gamma_1 + \gamma_2^t\Gamma\gamma_2 = \frac{1}{2}\gamma_1^t(\Gamma+\Gamma^t)\gamma_1 + \frac{1}{2}\gamma_2^t(\Gamma+\Gamma^t)\gamma_2 > 0,$$

where, $\gamma = \gamma_1 + \mathrm{i}\gamma_2$. □

Remark. As with the successive over-relaxation methods, the optimal values of the iteration parameters are known only if the matrices involved have special structure. Indicators of such special structures can be found in [14,15]. For the present work, this problem is still open. Corollary 2, however, provides a condition that is easy to check for the anticipation of the presence of an optimal value for the parameter. From an engineering point of view, however, the following guidelines seem to work very well.

1. For combinations of low values of the relative sizes of the BEM to FEM sub-domains, and high values of the relative stiffness of the BEM to FEM sub-domains, the relaxation parameters may be assigned a relatively low value.
2. For combinations of high values of the relative sizes of the BEM to FEM sub-domains, and low values of the relative stiffness of the BEM to FEM sub-domains, the applicable range of the relaxation parameters becomes wider.

Fortunately, most of the FEM/BEM coupling applications satisfy the second case and therefore, a wider range of the relaxation parameters is applicable to assure solution convergence.

We proceed to show that the conditions of Theorem 1 cannot be relaxed.

Proposition 3. *If the system* (37) *has a root λ such that $(a+b) > 0$ where a and b are given by* (40), *then the system is unstable for all positive values of ρ.*

Proof. First note that for any $z \in C$ and $o > 0$ we have $\mathrm{Re}\sqrt{z^2+\sigma} > \mathrm{Re}\, z$ where the branch $-\pi < \omega \leqslant \pi$ is taken for the square root function. Indeed to see this, write $z = x + \mathrm{i}y$, then

$$\mathrm{Re}\sqrt{z^2+\sigma} = \frac{\sqrt{(x^2-y^2+\sigma) + \sqrt{(x^2-y^2+\sigma)^2 + 4x^2y^2}}}{2} = \frac{\sqrt{(x^2-y^2+\sigma) + \sqrt{(x^2+y^2+\sigma)^2}}}{2}$$
$$= \sqrt{x^2+\sigma} \geqslant |x| \geqslant \mathrm{Re}\, z.$$

Applying this to Eq. (41) we get:

$$\mathrm{Re}\,\lambda^+ = \frac{(1-\rho\mathrm{Re}\, a) + \mathrm{Re}\sqrt{(1+\rho a)^2 - 4(a+b)}}{2} \geqslant \frac{1-\rho\mathrm{Re}\, a + \mathrm{Re}(1+\rho a)}{2} = 1.$$

Therefore $|\lambda^+| \geqslant 1$ and the system is unstable for all positive values of ρ. □

If the system (37) has a root λ such that $(a+b)<0$ then we conclude similarly, that the system is unstable for all negative values of ρ. Hence, the following corollary:

Corollary 3. *If the system* (37) *has two roots* λ_1, λ_2 *for which* $(a_1+b_1)(a_2+b_2)<0$ *where* a_1, b_1, a_2, b_2 *are given by* (40) *then the system is unstable for all values of* ρ.

5. Numerical examples

Conditions for convergence were established theoretically in Sections 3 and 4. In this section we apply the foregoing discussion with several example problems.

Consider the potential flow problem shown in Fig. 4. The two sub-domains Ω_B and Ω_F are governed by Laplace equation i.e., $k_i\nabla^2 u=0$ in Ω_i, $i=1,2$, where k_i is the material property in the sub-domain Ω_i. The domain is decomposed to the FEM and BEM sub-domains with $0\leqslant x\leqslant a$. The boundary conditions are selected as $u(0,y)=0$, $u(a,y)=200$, and zero flux ($k_i\nabla u$) elsewhere. The problem is investigated for different values of a_B/a_F and K_B/K_F (see, i.e., Fig. 5 which shows the discretization for $a_B/a_F=1$). Setting the values of a_B, a_F, K_B and K_F to unity, the problem is solved numerically using the three domain decomposition methods shown in Section 2. Table 1 gives the range and the optimum values for the relaxation

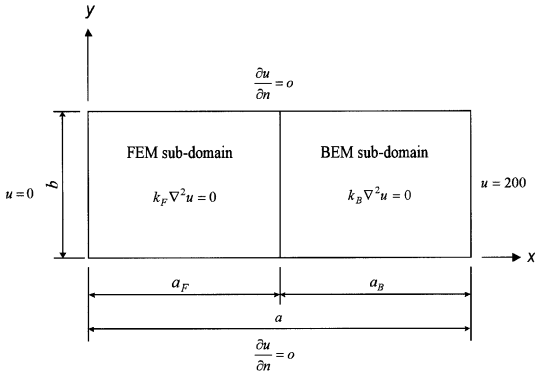

Fig. 4. Potential flow problem.

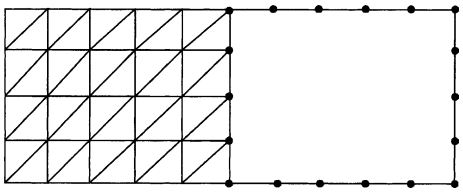

Fig. 5. Discretization of the potential flow problem.

Table 1
Numerical results for the potential flow problem with a_B, a_F, K_B and K_F set to unity

Scheme	Relaxation parameter	Range	Optimum
Parallel Neumann–Neumann	β	0–0.98	0.18
Parallel Dirichlet–Neumann	α	0–0.98	0.18
Sequential Dirichlet–Neumann	γ	0–0.98	0.5

Table 2
Applicable range for the potential flow problem and for different values of a_B/a_F and K_B/K_F

a_B/a_F		K_B/K_F		
		0.50	1.0	2.0
0.2	β	0.02–0.98	0.02–0.98	0.02–0.98
	α	0.02–0.36	0.02–0.18	0.02–0.08
	γ	0.02–0.56	0.02–0.32	0.02–0.18
1.0	β	0.02–0.98	0.02–0.98	0.02–0.98
	α	0.02–1.98	0.02–0.98	0.02–0.48
	γ	0.02–1.32	0.02–0.98	0.02–0.66
4.0	β	0.02–0.98	0.02–0.98	0.02–0.98
	α	0.02–2.28	0.02–2.66	0.02–1.98
	γ	0.02–1.76	0.02–1.56	0.02–1.32

parameters with a_B, a_F, K_B and K_F set to unity. Table 2 shows the applicable range of the relaxation parameters for the coupling schemes with different combinations of a_B/a_F and K_B/K_F. The optimum and limit values of the relaxation parameters are found in close agreement with the theoretical analysis given in Sections 3 and 4.

Now let us consider Fig. 6, where a steel cantilever beam is subjected to a uniform tensile loading of 20×10^3 units at its free end, and is considered to be in a state of plane stress with an elastic modulus, $E = 29 \times 10^6$ units, and a Poison's ratio $v = 0.3$. The beam is 20 units long and 10 units high, and is assumed to be weightless. The results obtained using the sequential Dirichlet–Neumann and the parallel Dirichlet–Neumann domain decomposition coupling methods and for the two meshes shown in Fig. 7 match very well with the analytical solutions. It should be mentioned over here that the problem cannot be solved using the parallel Neumann–Neumann domain decomposition coupling method as the Neumann boundary conditions are prescribed for the entire external boundary of the BEM sub-domain.

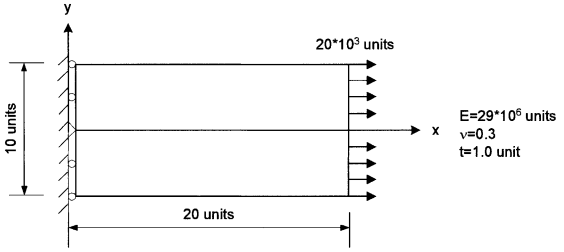

Fig. 6. Cantilever beam subjected to uniform loading.

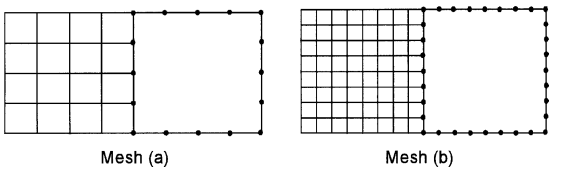

Fig. 7. FEM/BEM discretization for the cantilever beam problem.

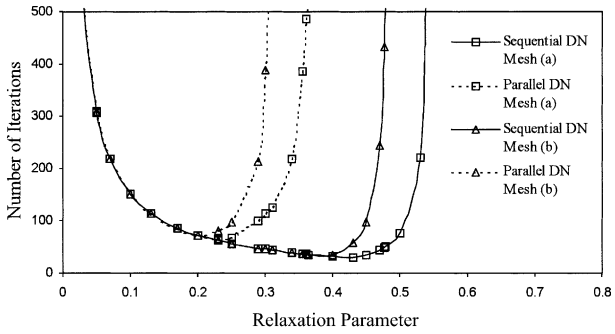

Fig. 8. Effect of the mesh density on solution convergence.

Fig. 8 illustrates the effect of the mesh size on the convergence of solution. For mesh (a), γ should be within the range of 0.02–0.54, whilst the range for α is 0.02–0.36. Beyond these values the sequential Dirichlet–Neumann and the parallel Dirichlet–Neumann domain decomposition coupling methods will not converge. The range from which the relaxation parameter to be chosen becomes narrower with a denser mesh of the computational sub-domains.

Using mesh (a) of Fig. 7, the problem is investigated for different relative values of modulus of elasticity for the BEM and FEM sub-domains, E_B/E_F. Fig. 9 indicates that as E_B/E_F decreases, the range from which the relaxation parameters to be chosen increases. The range for both γ and α reduces to very narrow ones for higher values of E_B/E_F. Table 3 shows the allowable range and the optimum values for the relaxation parameters and for different values of E_B/E_F.

For the cantilever beam problem, the optimum and limit values of γ and α are found in close agreement with the theoretical analysis given in Sections 3 and 4.

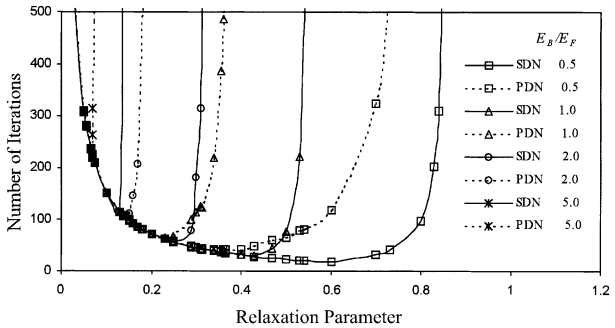

Fig. 9. Effect of the material properties of the sub-domains on solution convergence.

Table 3
Applicable range and optimum values for the cantilever beam problem and for different values of E_B/E_F

Relaxation parameter		E_B/E_F			
		0.50	1.0	2.0	5.0
γ	Range	0.02–0.85	0.02–0.54	0.02–0.31	0.02–0.14
	Optimum	0.6	0.43	0.25	0.13
α	Range	0.02–0.73	0.02–0.37	0.02–0.18	0.02–0.08
	Optimum	0.36	0.23	0.15	0.07

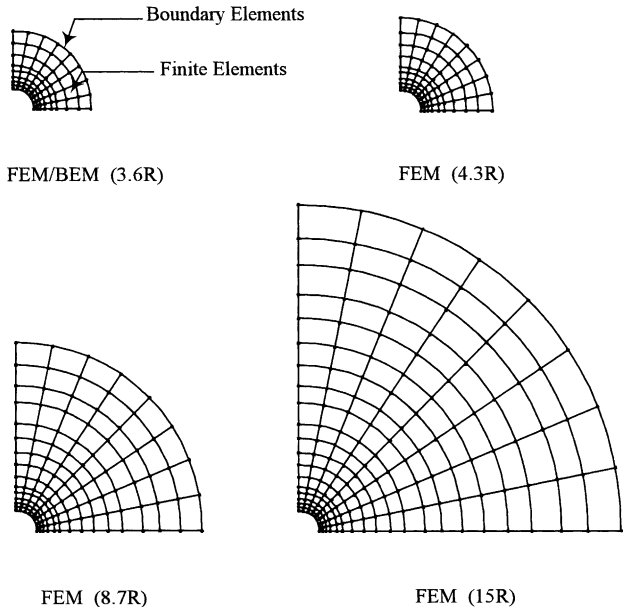

Fig. 10. FEM and FEM/BEM discretization for the tunnel problem.

Now let us consider another example where the excavation of a circular tunnel opening in a geological medium is analyzed. The tunnel is deeply inserted in an intact rock. The plane strain condition is assumed to prevail. The radius of the tunnel R is taken as 100 units. The material properties employed are as follows: Young's modulus $E = 2.1 \times 10^4$ units, Poisson's ratio $v = 0.18$, Cohesion $c = 10$ units and angle of internal friction $\phi = 41°$. First the excavation of tunnel is analyzed with the FEM. In this case the infinite domain is truncated at 4.3, 8.7 and 15 times the radius of the tunnel from the center of the tunnel opening. At the boundary of the tunnel, the forces corresponding to in situ state of stress condition are computed at the nodal points and applied in the opposite direction to simulate the excavation of the opening. The problem is then analyzed using the sequential Dirichlet–Neumann domain decomposition coupling method. The FEM/BEM interface is set at 3.6 times the radius of the tunnel. Due to symmetry only one quarter of the problem is modeled. Fig. 10 shows the discretization with the FEM and coupled FEM/BEM.

Figs. 11 and 12, respectively, show the radial displacements (u_r) and radial stresses (σ_r) by the FEM and FEM/BEM as compared to the closed form solution. For the FEM, it is observed that better accuracy is

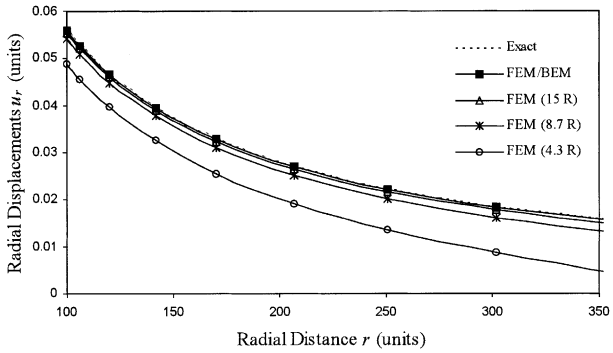

Fig. 11. Radial displacements for elastic analysis of the tunnel problem.

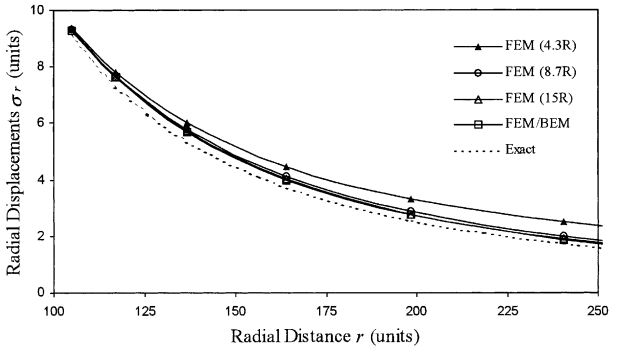

Fig. 12. Radial stresses for elastic analysis of the tunnel problem.

achieved as the extent of boundary distance increases. The FEM/BEM solutions give higher accuracy compared to the FEM. The results clearly show the advantage of using the FEM/BEM in terms of accuracy. In order to assure convergence, γ should be within the range of 0.02–1.03 with an optimum value of 0.59. The optimum and limit values of γ are in close agreement with the ones determined theoretically using the analysis given in Sections 3 and 4.

6. Conclusions

In this work, we investigate the convergence of three available domain decomposition-coupling schemes. Several example problems are also given. The theoretical analysis provides an interval from which the relaxation parameter has to be chosen. The choice of this parameter is essential to guarantee the convergence of the method.

References

[1] O.C. Zienkiewicz, D.W. Kelly, P. Bettes, The coupling of the finite element method and boundary solution procedures, International Journal for Numerical Methods in Engineering 11 (1977) 355–375.
[2] G. Beer, J.L. Meek, The coupling of boundary and finite element methods for infinite domain problems in elasticity, in: C.A. Brebbia (Ed.), Boundary Element Methods, Springer, Berlin, 1981, pp. 575–591.
[3] G. Swoboda, W. Mertz, G. Beer, Rheological analysis of tunnel excavations by means of coupled finite element (FEM)–boundary element (BEM) analysis, International Journal for Numerical and Analytical Methods in Geomechanics 11 (1987) 115–129.
[4] K. Kohno, T. Tsunda, H. Seto, M. Tanaka, Hybrid stress analysis of boundary and finite elements by super-element method, in: C.A. Brebbia, J.J. Conor (Eds.), Advances in Boundary Elements, vol. 3, Springer, Berlin, 1989, pp. 27–38.
[5] K.L. Leung, P.B. Zavareh, D.E. Beskos, 2-D elastostatic analysis by a symmetric BEM/FEM scheme, Engineering Analysis with Boundary Elements 15 (1995) 67–78.
[6] K. Kishimoto, I. Yamaguchi, M. Tachihara, M., S. Aoki, M. Sakata, Elastic–Plastic Fracture Mechanics Analysis by Combination of Boundary and Finite Element Methods, in: 5th World Conference on the Boundary Element Method, Hirohima, Japan, 1983, pp. 975–984.
[7] O. Kui, J. Zailu, The Elasto-Plastic Analysis of BEM and FEM in Structures Composed of Thin Plates, in: Proceedings of the 2nd China–Japan Symposium on Boundary Element Methods, Beijing, China, 1988, pp. 393–400.
[8] A. Varadarajan, K.G. Sharma, R.B. Singh, Elasto-plastic analysis of an underground opening by FEM and coupled FEBEM, International Journal for Numerical and Analytical Methods in Geomechanics 11 (1987) 475–487.
[9] N. Kamiya, H. Iwase, E. Kita, Parallel computing for the combination method of BEM and FEM, Engineering Analysis with Boundary Elements 18 (1996) 221–229.
[10] N. Kamiya, H. Iwase, BEM and FEM combination parallel analysis using conjugate gradient and condensation, Engineering Analysis with Boundary Elements 20 (1997) 319–326.

[11] C.-C. Lin, E.C. Lawton, J.A. Caliendo, L.R. Anderson, An iterative finite element–boundary element algorithm, Computers & Structures 39 (1996) 899–909.
[12] Y.T. Feng, D.R.J. Owen, Iterative solution of coupled FE/BE discretization for plate-foundation interaction problems, International Journal for Numerical Methods in Engineering 39 (1996) 1889–1901.
[13] J. Stoer, R. Bulirsch, Introduction to Numerical Analysis, Springer-Verlag, Berlin, 1980.
[14] R.S. Varga, Matrix Iterative Analysis, Series in Automatic Computation, Prentice Hall, Englewood Cliffs, 1962.
[15] D.M. Young, Iterative Solution of Large Linear Systems, Computer Science and Applied Mathematics, Academic Press, NY, 1971.